Droop Control for a Multi-Line Current Flow Controller in Meshed Multi-Terminal HVDC Grid Under Large DC Disturbances

Wang, Puyu; Deng, Na; Zhang, Xiao-ping

DOI:
10.1109/JPETS.2018.2842041

Received 22 August 2017; revised 11 January 2018; accepted 9 May 2018.
Date of publication 1 June 2018; date of current version 22 June 2018.

Digital Object Identifier 10.1109/JPETS.2018.2842041

Droop Control for a Multi-Line Current Flow Controller in Meshed Multi-Terminal HVDC Grid Under Large DC Disturbances

PUYU WANG[1,2] (Member, IEEE), NA DENG[3], AND XIAO-PING ZHANG[4] (Senior Member, IEEE)

[1]Department of Electrical Engineering, School of Automation, Nanjing University of Science and Technology, Nanjing 210094, China
[2]Jiangsu Collaborative Innovation Center for Smart Distribution Network, Nanjing Institute of Technology, Nanjing 211167, China
[3]ABB (China) Ltd., Nanjing 210005, China
[4]Department of Electronic Electrical and Systems Engineering, School of Engineering, University of Birmingham, Birmingham B15 2TT, U.K.

CORRESPONDING AUTHOR: X.-P. Zhang (x.p.zhang@bham.ac.uk)

This work was supported in part by EPSRC, U.K., under Grant EP/K006312/1, in part by the China Scholarship Council & Si-Guang Li Scholarship, in part by the Department of EESE, School of Engineering, University of Birmingham, in part by the Fundamental Research Funds for the Central Universities under Grant 30917011330, in part by the Open Research Fund of Jiangsu Collaborative Innovation Center for Smart Distribution Network under Grant XTCX201704, in part by the National Natural Science Foundations of China under Grant 51577092, in part by the Global Energy Interconnection Research Institute Europe under Grant SGRIZLKJ(2015) 214, and in part by the Natural Science Foundation of Jiangsu Province.

ABSTRACT The security, stability, and reliability of power supply are essential and must be guaranteed during operation of multi-terminal HVDC (MTDC) grids, particularly under disturbances, such as a line or converter loss, on the dc grid side. In this paper, a multi-line current flow controller (CFC) is expanded from the existing two-line CFC for meshed MTDC grids with two main contributions: a droop control scheme for a multi-line CFC, which is capable of coordinating dc line current/power sharing under large dc disturbances is proposed and a selection method for the droop gains is proposed. The multi-line CFC with the droop control scheme proposed can achieve full controllability of the currents among multiple dc lines and the security and continuity of power supply of the unfaulty dc lines can be guaranteed. The stability and dynamic performance of the droop controller can both be satisfied with the proposed selection method. The effectiveness of the proposed scheme and selection method is justified by RTDS simulations. The proposed scheme is simple and easy to implement. The proposed dynamic simulation-based selection method has the flexibility suiting both online and offline calculation tools and the consideration of system nonlinear characteristics and control limits/constraints.

INDEX TERMS Droop control, droop gain selection method, multi-line current flow controller (CFC), meshed HVDC grid, dc grid security and stability, RTDS.

I. INTRODUCTION

Voltage source converter (VSC) based HVDC has two categories, point-to-point and multi-terminal configurations. For multi-terminal HVDC (MTDC) grids [1]–[5], they have two main topologies: radial topology and meshed topology. In comparison with the radial topology, the meshed topology is considered to have better DC line utilization, lower capital costs, higher reliability and flexibility [3]–[5]. In a meshed MTDC grid, deviations of DC line current may be regulated within an operational range via proper tuning of the control parameters of the voltage source converters (VSCs) at each DC terminal [5]. However, the exact division of the branch currents on the DC lines depends on the network topology, terminal voltage differences, and transmission line resistance, which indicates that the branch currents are not fully controllable [6]. In addition, considering meshed MTDC grids under disturbance conditions, e.g. an outage of a DC line or a sudden loss of a DC terminal, the remaining DC lines may become overloaded, including the extreme condition, i.e. the overall system may collapse. Therefore, an effective approach which can achieve flexible and emergency current/power control for meshed MTDC grids deserve research and exploration.

Power flow control of AC power grids using FACTS devices has been comprehensively investigated [7]. For the power flow control of MTDC grids, droop control has been predominantly utilized in comparison with the master-slave

control due to its power sharing capability and coordination among multiple terminals, i.e. the functionality of coordinating the control of both the DC voltage and active power [4], [5], [8]–[12]. In [11], an improved analytical model, which was derived by the bisection algorithm and superposition principle, was proposed to estimate the system performance under the conditions of converter outages and converter overloading. In [12], a new droop control controller structure was proposed and it could maintain the DC nominal voltage under faults or converter disconnection, while preserving the power flow in the DC grid. However, the method was only justified in an MTDC grid in radial topology.

The use of droop control on the VSCs can only regulate the power at the converter DC terminals, while power flow control within the DC grids has not been fully investigated and is considered to be a new and popular area [13]–[31]. Three types of control devices that have DC power flow control capability have been proposed so far [13]–[31], namely variable resistor [13], [14], DC-DC converter [15]–[20], and series voltage source [21]–[31]. The first method is by inserting variable resistance into a DC line. The DC branch currents presented in [13] and [14] were well regulated by switching on and off variable resistance of the power electronics device and thereby changing the DC line resistance. However, the power losses due to the switch-in resistance were the main disadvantage. The second method is by means of a DC-DC converter with several different topologies being proposed [15]–[20]. However, the requirement of using DC-DC converters is that they need to withstand high voltage and power, which results in high power losses and construction cost. The third method is by inserting an equivalent voltage source into a DC line to regulate the power/current flow [21]–[31]. In comparison with the first two methods, i.e. using an inserted variable resistor or a DC-DC converter, the third method, i.e. using a variable voltage source, has lower power losses, lower requirement on the voltage rating, and can be easily implemented [9], [21].

Among the existing approaches of adopting variable voltage source for DC power flow control, a connection with an external AC voltage source to export/import power from/to the DC grid was commonly used in previous schemes [22]–[25]. Proposals of DC power flow controller (PFC)/current flow controller (CFC) with simple circuit topologies could achieve the same functionality while without the need of external AC or DC voltage source[26]–[31] An interline DC power flow controller (IDCPFC) was proposed in [26]. The proposed IDCPFC had no requirement on external power source and could achieve power flow control in a meshed 3-terminal HVDC grid. An m-port DC power flow controller (MDCPFC), which could generator incremental DC voltages for DC power flow control without requiring power exchange with an external AC network, was proposed in [27]. However, the requirement of AC transformers increased the total cost and space in the MDCPFC. A cascaded power flow controller (CPFC) with a two-layer control strategy was proposed in [28]. The proposed CPFC could reschedule the power flow to enhance the utilization of DC lines in an MTDC grid. However, the proposed CPFC was based on controlled current and voltage source, i.e. detailed topology of the CPFC was not provided. In [29]–[31], the use of a DC CFC with two full-bridge converters which interconnected by a common capacitor for energy exchange was proposed. The CFC proposed in [26]–[31] was mainly applied in the simplest 3-terminal meshed HVDC grid with a two-line CFC. For a meshed MTDC grid with a more complex topology and multiple DC lines connected at one terminal, e.g. the MTDC grid shown in Fig. 1, a multi-line CFC would be needed for the multi-branch current regulation. In addition, the security, stability and reliability of power supply are essential, particularly under disturbances. Furthermore, although the DC CFC proposed in previous literature could achieve adjustment of DC line currents [26]–[31] in meshed MTDC grids, the coordination of DC line currents might not be well controlled under disturbances and the concept of applying droop control in the multi-line CFC for DC power flow control in meshed MTDC grids has never been proposed yet.

In this paper, apart from achieving the capability of providing current flow control among multiple DC lines, a generalized multi-line CFC is developed and expanded from the existing two-line CFC [29]–[31] for meshed DC grids with the following major contributions: (1) A coordinated droop control scheme is proposed for the current/power sharing within the CFC, particularly under large disturbances such as an outage of a DC line or a sudden loss of a DC terminal. Thus, the security and continuity of power supply of the unfaulty DC lines can be guaranteed. (2) A selection method for the droop gains is proposed to satisfy both stability and dynamic requirements. The proposed selection method has the flexibility suiting both online and offline calculation tools. Due to the fact that the focus of this study is on the DC side of the MTDC grid, the converter AC grid or MMC dynamics are not included.

The rest of the paper is arranged as follows. Modelling of a generalized meshed MTDC grid is derived in Section II. The topology and mathematical model of a multi-line CFC are also presented. A coordinated droop control scheme for the multi-line CFC is proposed and comprehensively discussed in Section III. In Section IV, the selection method for the droop gains is analyzed. Simulation and study results are demonstrated in Section V and several conclusions are drawn in Section VI. More information regarding the modelling of the meshed MTDC grid with multi-line CFC and the droop gain selection method is provided in the Appendix.

II. MESHED MTDC GRID AND MULTI-LINE CFC

A. A GENERALIZED MESHED MTDC GRID

In this section, the mathematical model of a generalized meshed MTDC grid is derived. Fig. 1 shows a schematic representation of a generalized meshed MTDC grid.

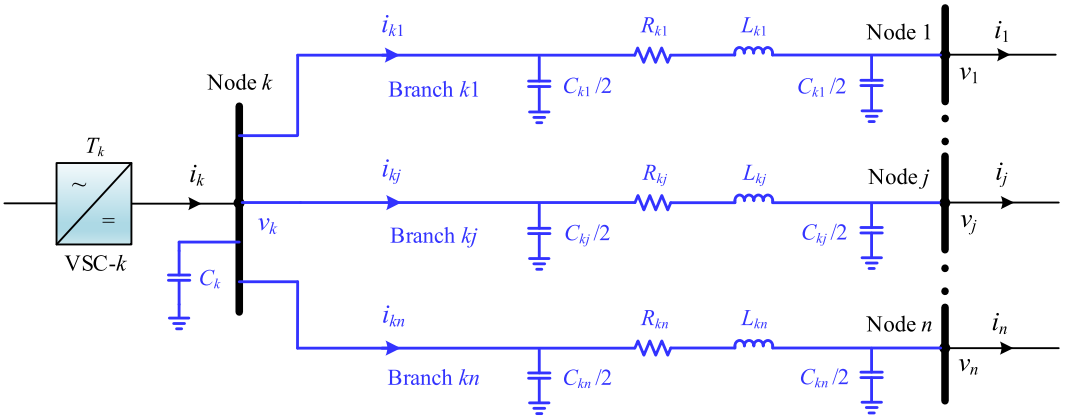

FIGURE 1. **Schematic description of a generalized meshed MTDC grid.**

In Fig. 1, T_k denotes a terminal of the MTDC system; VSC-k denotes the converter station at T_k. The AC side of the VSC is connected with an AC power source, while the DC side of VSC is connected with the meshed MTDC grid. In the MTDC grid, there are intermediate nodes, which are convergence points of multiple DC branches/lines. The branch between Node k and Node j is denoted as B_{kj}. All the DC branches/lines are modelled by lumped π-section circuits [31], [37], [38]. The relationship of the voltages and currents for the branches connected at Node k can be derived as follows:

$$L_{kj}\frac{di_{kj}}{dt} = v_k - v_j - R_{kj}i_{kj} \quad j = 1\ldots n \tag{1}$$

$$C_k\frac{dv_k}{dt} = i_k - \sum_{j=1}^{n} i_{kj} \tag{2}$$

All the branch voltage/current equations can be combined to form the compact state-space expression:

$$\dot{\mathbf{x}} = \mathbf{A}\mathbf{x} + \mathbf{B}\mathbf{u} \tag{3-a}$$

$$\mathbf{y} = \mathbf{C}\mathbf{x} + \mathbf{D}\mathbf{u} \tag{3-b}$$

where $\mathbf{x}$ is the state vector, which consists of the node voltages and branch currents. $\mathbf{u}$ is the input vector, which consists of the terminal voltages and currents.

B. MULTI-LINE CURRENT FLOW CONTROLLER

A multi-line CFC, which comprises three or more DC-DC bridge converters working together to control the DC branch/line currents in the MTDC grid, is developed and expanded from the existing two-line CFC [29]–[31]. The simplest multi-line CFC consists of three DC-DC converters and can provide current control over three branches. The structure of a generalized multi-line CFC in a meshed MTDC is depicted in Fig. 2(a). The detailed structure of the multi-line CFC is shown in Fig. 2(b).

The multi-line CFC is installed at T_k with n branches which connect to the nodes at other terminals. It consists of three or more identical DC-DC bridge converters, namely sub-modules (SM-kj, $j = 1, \ldots, n$) in Fig. 2, that share a common capacitor. The common capacitor of the CFC works as a power exchange hub of the DC-DC converters. Each DC-DC converter has four identical switches where each switch consists of an insulated-gate bipolar transistor (IGBT) and an anti-parallel diode.

In order to achieve fast and effective control of the DC-DC converters, the pulse width modulation (PWM) strategy is applied to generate the firing signals [32]. The control of the DC-DC converters is similar, taking the DC-DC converter (SM-kj) on Branch kj ($j = 1, \ldots, n$) with four switches S_{hkj} ($h = a, \ldots, d$) as an example. The position of the four switches S_{hkj} are shown in Fig. 2. S_{akj} and S_{bkj} are triggered complementarily; similarly, S_{ckj} and S_{dkj} are triggered complementarily. Hence, the duty cycles of these switches, d_{hkj}, have a relationship defined as follows:

$$d_{akj} + d_{bkj} = 1 \tag{4-a}$$

$$d_{ckj} + d_{dkj} = 1 \tag{4-b}$$

In principle, different control schemes can be developed. In our current control scheme, the control status of S_{akj} and S_{bkj} is fixed, i.e. d_{akj} and d_{bkj} are set as constant values (d_{ak} and d_{bk}). However, d_{ckj} and d_{dkj} are variable and can be controlled. Table 1 summarizes the switching modes for the DC-DC converter on Branch kj. Each DC-DC converter has four switching modes, m_{kji} ($i = 1, \ldots, 4$), per cycle according to the combinations of the switches. In Mode 1, S_{akj} and S_{ckj} are switched on; In Mode 2, S_{akj} and S_{dkj} are switched on; In Mode 3, S_{bkj} and S_{ckj} are switched on; In Mode 4, S_{bkj} and S_{dkj} are switched on. In (4), d_{hkj} is the duty cycle of each switch, while a_{kji} is the duty cycle of the DC-DC converter under a current switching mode m_{kji}; e_{kji} is the voltage between Node$k$ and Node j'; i_{kji} is the DC branch/line current on Branch kj; u_{ck} is the voltage across the common capacitor C_{cfc}; i_{ckj} is the current through the common capacitor.

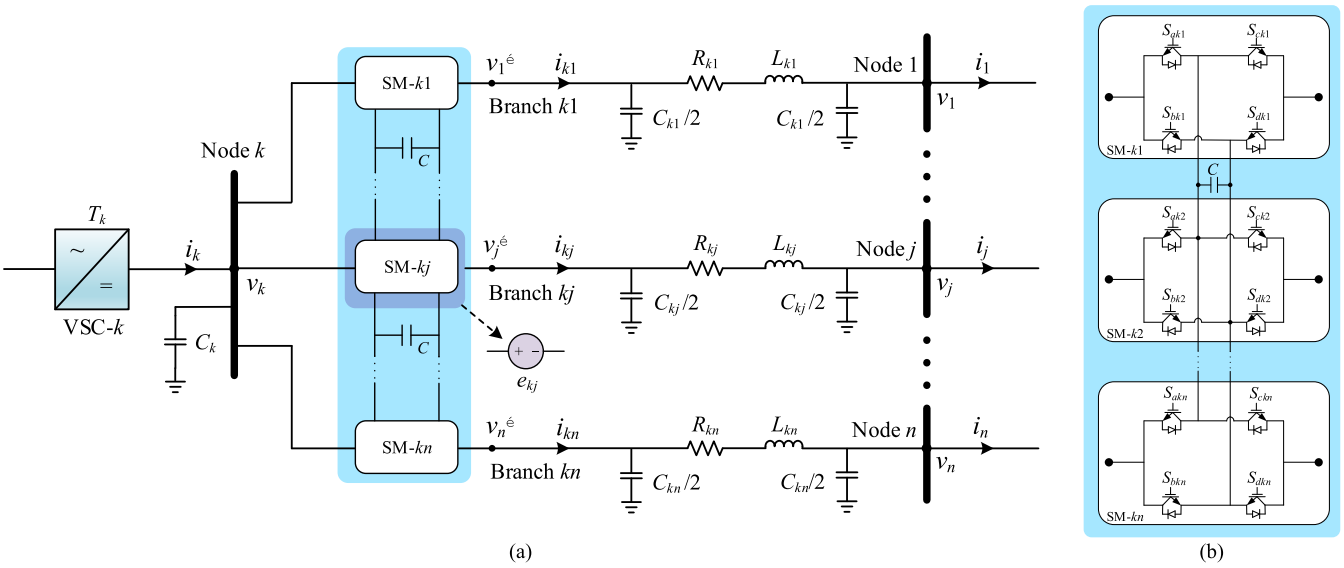

FIGURE 2. **Detailed structure of a multi-line CFC.**

TABLE 1. **Switching modes of DC-DC converter on branch *kj*.**

Switching Mode (m_{kji})	Switches 'ON'	Duty Cycle (a_{kji})	e_{kji}	i_{kji}
1	S_{akj}, S_{ckj}	a_{kj1}	0	0
2	S_{akj}, S_{dkj}	a_{kj2}	u_{ck}	i_{ckj2}
3	S_{bkj}, S_{ckj}	a_{kj3}	-u_{ck}	-i_{ckj3}
4	S_{bkj}, S_{dkj}	a_{kj4}	0	0

According to the switching characteristics of the DC-DC converter under four switching modes, the relationship between the duty cycle of the DC-DC converter a_{kji} and the duty cycle of the switches $d_{hk(j)}$ can be derived in (5):

$$a_{kj1} = \min\left\{d_{ckj}, d_{ak}\right\} \quad a_{kj2} = \max\left\{0, d_{ak} - d_{ckj}\right\} \quad \text{(5-a)}$$

$$a_{kj3} = \max\left\{0, d_{ckj} - d_{ak}\right\} \quad a_{kj4} = 1 - \max\left\{d_{ak}, d_{ckj}\right\} \quad \text{(5-b)}$$

Analyzing the voltage characteristics of the DC-DC converter under different switching modes, the relationship between e_{kj} and u_{ck} can be obtained:

$$e_{kj} = \sum_{i=1}^{4} a_{kji}\, e_{kji} = (d_{ak} - d_{ckj})u_{ck} \quad (6)$$

It shows that the DC-DC converter can be regarded as a voltage source to the DC branch/line where it is installed as shown in Fig. 2. The magnitude of the voltage between Node$k$ and Node j', e_{kj}, is related with the duty cycles of the switches and the magnitude of the common capacitor, u_{ck}. The expression of u_{ck} can be obtained by considering the charging and discharging currents of all the DC-DC converters constituting the multi-line CFC:

$$C\frac{du_{ck}}{dt} = i_{ck} = \sum_{j=1}^{n}(\sum_{i=1}^{4} a_{kji}\, i_{ckji}) = \sum_{j=1}^{n}(d_{ak} - d_{ckj})i_{ckj} \quad (7)$$

During the operation, the voltage of the common capacitor should be stable and remain controlled under acceptable limits, which is similar to the control principle of a two-line CFC [30], [31].

C. MESHED MTDC GRID WITH MULTI-LINE CFC

In this section, the mathematical model of the generalized meshed MTDC grid with the multi-line CFC is derived. For the sake of simplicity, it is assumed that only one multi-line CFC is installed at T_k.

The installation of the multi-line CFC brings an equation, which defines the relationship between the voltage of the common capacitor u_{ck} and the branch current i_{ckj}, i.e. (7). Apart from that, the installation of the multi-line CFC also has an impact on the modelling of the meshed MTDC grid. Due to the fact that the DC-DC converter of the multi-line CFC is equivalent to a voltage source to the branch where it is installed, the equation derived in (1) for Branch kj can be revised as follows:

$$L_{kj}\frac{di_{kj}}{dt} = v_k - e_{kj} - v_j - R_{kj}i_{kj} \quad (8)$$

where e_{kj} is given in (6).

Following the procedures above, the mathematical model of a generalized meshed MTDC grid with a multi-line CFC at Node k can be derived. If multiple multi-line CFCs are installed in a meshed MTDC, similar modelling procedures can be applied to derive the system characteristic equations.

The state-space equations for the meshed MTDC grid with the installation of a multi-line CFC at Node k can be

expressed as follows:

$$\begin{aligned}\dot{\mathbf{x}}_1 &= \mathbf{A_1 x_1} + \mathbf{Bu} \\ \mathbf{y_1} &= \mathbf{C_1 x_1} + \mathbf{Du}\end{aligned} \tag{9}$$

where $\mathbf{x_1}$ is the new state vector, which consists of the state vector $\mathbf{x}$ plus a new state variable u_{ck}, i.e. $\mathbf{x_1}$=[$\mathbf{x}$, u_{ck}].

III. CONTROL METHODOLOGIES FOR THE MULTI-LINE CFC

The fundamental objective of installing a multi-line CFC is to regulate the current of the DC branch/line where it is installed. The current regulation of the multi-line CFC is one of the control objectives and is realized via power exchange among the DC-DC converters, by charging and discharging the common capacitor. Under steady state conditions, it is considered that the power within the CFC is well balanced with the voltage across the common capacitor being well maintained [30], [31]. Hence, the other control objective is to maintain the voltage across the common capacitor. Based on the control objectives, two control methodologies with detailed means of implementation are proposed to be used for the control of a multi-line CFC; namely, basic current flow control and the coordinated droop control.

A. BASIC CURRENT FLOW CONTROL

The basic current flow control as depicted in Fig. 3, is similar to the control algorithm for a two-line CFC [19], which mimics the control principle of the master-slave control of VSC-HVDC systems. That is, one DC-DC converter of the CFC controls the DC voltage on the common capacitor, while the remaining DC-DC converters control the DC currents on the corresponding branches/lines.

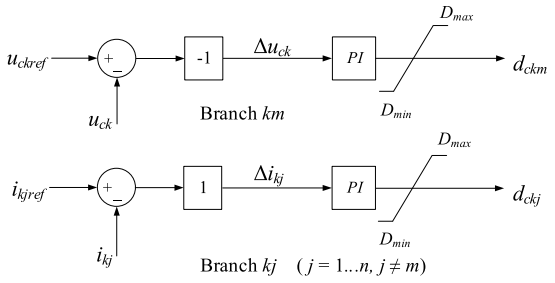

FIGURE 3. Basic current flow control.

For the DC-DC converter on Branch km, the measurement of the capacitor voltage u_{ck} is compared with the voltage reference u_{ckref} as shown in Fig. 3. The error signal Δu_{ck} passes through a *PI* controller to obtain the duty cycle d_{ckm}, which is then used for generating the firing signal for the switch, S_{ckm}. Thus, the voltage across the common capacitor is regulated by the DC-DC converter on Branch km. For the remaining DC-DC converters on the other branches, namely, Branch $kj(j = 1,\ldots,n, j \neq m)$, the measurement of the branch current i_{kj}, is compared with current reference i_{kjref}. The error signal Δi_{kj} passes through a *PI* controller to obtain the duty cycle d_{ckj} , which is then used for generating the firing signal for the switch, S_{ckj}. Thus, the current on Branch kj is controlled by the DC-DC converter on Branch kj.

B. COORDINATED DROOP CONTROL

Apart from the basic current flow control, an improved coordinated droop control scheme is proposed in this paper. In comparison with the basic current flow control, a key difference is that the regulation of the voltage across the common capacitor is not realized by a single DC-DC converter but is shared by all DC-DC converters. All the DC-DC converters contribute to the regulation of the voltage across the common capacitor, while the participation degree of each DC-DC converter is different. The participation degree is determined by the droop gain selection.

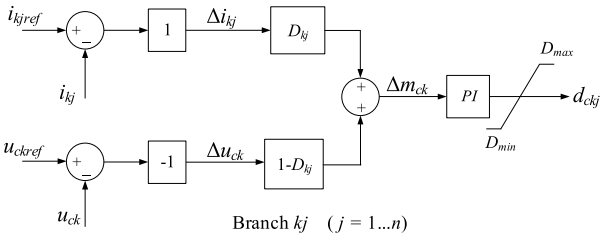

FIGURE 4. Coordinated droop control.

The coordinated droop control for the multi-line CFC is illustrated in Fig. 4. For the DC-DC converter on Branch kj the measurement of the branch current i_{kj}, is compared with current reference i_{kjref}. Meanwhile, the measurement of the capacitor voltage u_{ck} is compared with the voltage reference u_{ckref}. The current error Δi_{kj} is scaled by droop gain D_{kj} and is summed with the signal, which is generated by scaling of Δu_{ck} with the coefficient (1-D_{kj}). The addition result passes through a *PI* controller to obtain the duty cycle d_{ckj}, which is then used for generating the firing signal for the switch, S_{ckj}. Thus, the regulation of the branch currents and the capacitor voltage are performed by all DC-DC converters. According to Fig. 4, the following equations can be derived for the DC-DC converter on Branch kj:

$$\Delta i_{kj} = i_{kjref} - i_{kj} \tag{10-a}$$

$$\Delta u_{ck} = u_{ck} - u_{ckref} \tag{10-b}$$

$$\Delta i_{kj} D_{kj} + \Delta u_{ck}(1 - D_{kj}) = \Delta m_{kj} \tag{10-c}$$

Combining the equations of all DC-DC converters, we have:

$$\Delta \mathbf{x_{ck}} = \mathbf{x_{ckref}} - \mathbf{x_{ck}} \tag{11-a}$$

$$\mathbf{E}\Delta \mathbf{x_{ck}} = \Delta \mathbf{m_{ck}} \tag{11-b}$$

where $\mathbf{x_{ckref}}$ is the vector reference, $\mathbf{x_{ck}}$ is the feedback vector, $\Delta \mathbf{x_{ck}}$ is the error signal vector, $\Delta \mathbf{m_{ck}}$ is the error signal vector timing the droop weighting matrix $\mathbf{E}$. The expressions of

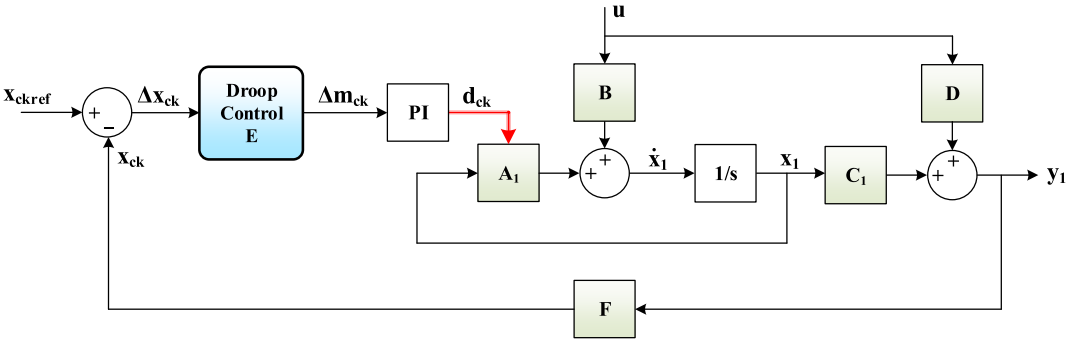

FIGURE 5. **Mathematical model of meshed MTDC grid with multi-line CFC.**

$\mathbf{x_{ckref}}$, $\mathbf{x_{ck}}$, $\Delta\mathbf{x_{ck}}$ and $\Delta\mathbf{m_{ck}}$ are as follows:

$$\mathbf{x_{ckref}} = \begin{bmatrix} i_{k1ref} & i_{kjref} & \dots & i_{knref} & -u_{ckref} \end{bmatrix}^T$$
$$\mathbf{x_{ck}} = \begin{bmatrix} i_{k1} & i_{kj} & \dots & i_{kn} & -u_{ck} \end{bmatrix}^T$$
$$\Delta\mathbf{x_{ck}} = \begin{bmatrix} \Delta i_{k1} & \Delta i_{kj} & \dots & \Delta i_{kn} & \Delta u_{ck} \end{bmatrix}^T$$
$$\Delta\mathbf{m_{ck}} = \begin{bmatrix} \Delta m_{k1} & \Delta m_{kj} & \dots & \Delta m_{kn} \end{bmatrix}^T$$

$\mathbf{E}$ is a n by $(n+1)$ matrix combining all the droop gains of the DC-DC converters:

$$\mathbf{E} = \begin{bmatrix} D_{k1} & 0 & 0 & \dots & 1-D_{k1} \\ 0 & D_{kj} & 0 & \dots & 1-D_{kj} \\ \dots & \dots & \dots & \dots & \dots \\ 0 & 0 & \dots & D_{kn} & 1-D_{kn} \end{bmatrix}$$

The proposed coordinated droop control scheme has two main benefits:

- Firstly, the multi-line CFC with coordinated droop control can be deployed to limit transient overcurrents on the DC branches/lines. This is due to the fact that any changes of current on a DC branch/line will immediately reflect on the change of the capacitor voltage; thus, the other branches that connect with the multi-line CFC can swiftly detect this change and share the changes of the current on the DC branch/line.
- Secondly, the multi-line CFC with coordinated droop control may maintain the capacitor voltage and present satisfactory performance of branch current regulation under small disturbances or even extreme conditions. This is because the regulation of the capacitor voltage is shared by all DC-DC converters. Under extreme conditions, e.g. one DC branch/line is suddenly disconnected, the capacitor voltage may still be maintained by the other DC-DC converters on the remaining branches/lines and the whole system may be able to ride through the extreme condition with satisfactory regulation of the capacitor voltage and branch currents.

IV. DROOP GAIN SELECTION

The mathematical model of the DC grid is depicted in Fig. 5. In Fig. 5, $\mathbf{A_1}$, $\mathbf{B}$, $\mathbf{C_1}$ are the same as those in (9). $\mathbf{F}$ is the feedback matrix. Through the comparison of the vector reference $\mathbf{x_{ckref}}$ with the feedback vector $\mathbf{x_{ck}}$, the obtained error signal vector $\Delta\mathbf{x_{ck}}$ are weighted by the droop gain matrix $\mathbf{E}$. The duty cycle signals, $\mathbf{d_{ck}}$, are obtained after the *PI* controllers. It can be derived from (6)–(9) that the state matrix $\mathbf{A_1}$ is closely related to the duty cycle $\mathbf{d_{ck}}$. Thus, the state matrix $\mathbf{A_1}$, which has an impact on the overall system stability and dynamics, can be dynamically adjusted by the control of $\mathbf{d_{ck}}$, the results of which are closely related with the selection of the droop control matrix $\mathbf{E}$. Hence, the selection of the droop gains has great impact on the performance of the multi-line CFC and the overall MTDC system.

According to aforementioned analysis, a proper selection of the droop gain matrix $\mathbf{E}$ can influence the results of $\mathbf{d_{ck}}$, which will proceed to impact on the state matrix $\mathbf{A_1}$. In order to attain an appropriate range of droop gains, it is essential to obtain the relationships of the droop gain matrix $\mathbf{E}$, duty cycle $\mathbf{d_{ck}}$ and state matrix $\mathbf{A_1}$. Based on the mathematical model in Fig. 5, the following equality constraints can be obtained:

$$\mathbf{A_1 x_1} + \mathbf{B u} = \dot{x}_1 \tag{12-a}$$
$$\mathbf{E}\left(\mathbf{x_{ckref}} - \mathbf{x_{ck}}\right)\left(\mathbf{P} + \int \mathbf{I} dt\right) = \mathbf{d_{ck}} \tag{12-b}$$
$$\mathbf{F C_1 x_1} = \mathbf{x_{ck}} \tag{12-c}$$

where (12-b) signifies the relationship between $\mathbf{E}$ and $\mathbf{d_{ck}}$, while the relationship between $\mathbf{d_{ck}}$ and $\mathbf{A_1}$ can be directly obtained in (9). A complete representation of (9) is presented in (20) in the Appendix where it is clearly shown that the duty cycle $\mathbf{d_{ck}}$ is included in the state matrix $\mathbf{A_1}$.

In order to solve (12-b) so as to obtain proper sets of droop gains, a scanning method, i.e. a specific step is chosen for the selection of the droop gains between a certain range, say [0, 1] to evaluate if the selected droop gains satisfy predefined constraints, is utilized for the iterative calculation. However, the main challenge of the calculation is that the control variable $\mathbf{x_{ck}}$ is a function of the state variable $\mathbf{x_1}$ whereas $\mathbf{x_1}$ is a function of $\mathbf{d_{ck}}$, which also appears on the right-side of the equation. In order to solve this challenge, Heun's method [33]–[34] is used. The application of Heun's method and the main process for the selection of droop gains are summarized as follows with an overall flowchart illustrated in Fig. 6.

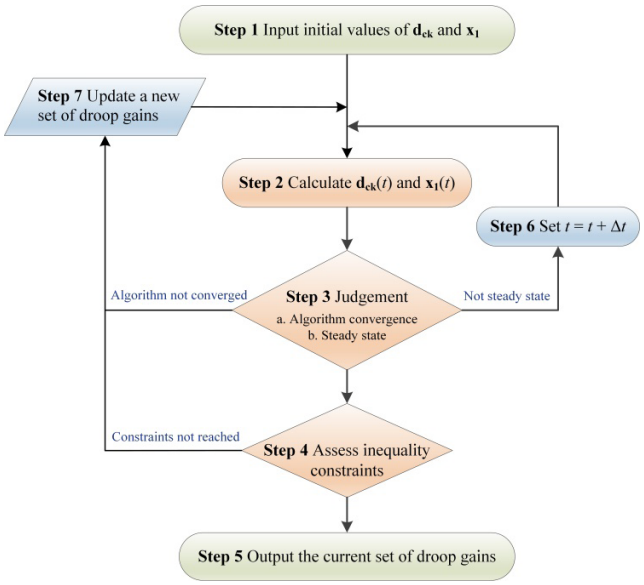

FIGURE 6. **Flowchart of the method for droop gain selection.**

Step 1: Input $\mathbf{d}_{\mathbf{ck}}^{(0)}$, $\mathbf{x}_{\mathbf{1}}^{(0)}$, $\mathbf{x}_{\mathbf{ckref}}$, maximum number of iterations N_{max}, maximum time T_{max} allowed for the MTDC grid to reach a steady state. The state variables and controlled inputs of the MTDC grid are set to the steady state condition while the state variables of the CFC controller are set to zero. This step is to initialize the iterative selection process when the MTDC grid has reached the steady state with the CFC being bypassed.

Step 2: Iteratively calculate $\mathbf{d}_{\mathbf{ck}}^{(n)}(t)$ and $\mathbf{x}_{\mathbf{1}}^{(n)}(t)$.

Combine the equality constraints (12-b) and (12-c):

$$\mathbf{d_{ck}}(t) = \mathbf{P} \cdot f(\mathbf{d_{ck}}(t)) + \mathbf{I} \int_{-\infty}^{t} f(\mathbf{d_{ck}}(\tau)) d\tau \tag{13}$$

where

$$f(\mathbf{d_{ck}}(t)) = \mathbf{E}\left(\mathbf{x_{ckref}} - \mathbf{FC_1 x_1}\left(\mathbf{d_{ck}}(t)\right)\right)$$

In order to conduct iterative calculations, $\mathbf{x_1}(\mathbf{d_{ck}}(t))$ is derived by re-writing (12-a) into the discrete form as follows:

$$\frac{\mathbf{x_1}(t) - \mathbf{x_1}(t - \Delta t)}{\Delta t} = \mathbf{A_1}(t)\mathbf{x_1}(t) + \mathbf{Bu}(t) \tag{14}$$

Thus, we can have the iterative equation for $\mathbf{x_1}(t)$:

$$\mathbf{x}_{\mathbf{1}}^{(n)}(t) = (\mathbf{I} - \Delta t \cdot \mathbf{A}_{\mathbf{1}}^{(n)}(t))^{-1} \cdot (\mathbf{x_1}(t - \Delta t) + \Delta t \cdot \mathbf{Bu}(t)) \tag{15}$$

where n is the iterating count.

In order to solve $\mathbf{d_{ck}}(t)$ in (13), Heun's method [33]–[34] is used. Considering the initial condition:

$$\mathbf{d}_{\mathbf{ck}}^{(0)}(t) = \mathbf{d_{ck}}(t - \Delta t) + \mathbf{I}\Delta t \cdot f(\mathbf{d_{ck}}(t - \Delta t)) \tag{16}$$

Using the iterative equation of Heun's method [33]–[36]:

$$\mathbf{d}_{\mathbf{ck}}^{(n+1)}(t) = \mathbf{d_{ck}}(t - \Delta t) + (-\mathbf{P} + \frac{\mathbf{I}}{2}\Delta t) \cdot f(\mathbf{d_{ck}}(t - \Delta t)) + (\mathbf{P} + \frac{\mathbf{I}}{2}\Delta t) \cdot f(\mathbf{d}_{\mathbf{ck}}^{(n)}(t)) \tag{17}$$

Step 3: The relationship of **Step 3** with **Step 4**, **6** and **7** is shown in Table 2.

TABLE 2. **Relationship of step 3 with step 4, 6 and 7.**

From **Step 3**	If (18-b) is reached	If (18-b) is not reached
If (18-a) is reached	Go to **Step 4**	Go to **Step 6**
If (18-a) is not reached	Go to **Step 7**	

The convergence criteria of iterations is defined as:

$$\left|\mathbf{d}_{\mathbf{ck}}^{(n+1)}(t) - \mathbf{d}_{\mathbf{ck}}^{(n)}(t)\right| \leq \varepsilon_1 \quad n \leq N_{\max}\ t \leq T_{\max} \tag{18-a}$$

The criteria of reaching steady state is defined as:

$$|\mathbf{d}_{ck}(t) - \mathbf{d}_{ck}(t - \Delta t)| \leq \varepsilon_2 \quad t \leq T_{\max} \tag{18-b}$$

Step 4: Assess whether inequality constraints are satisfied. The inequality constraints are defined as:

$$\begin{cases} \mathbf{x}_1 \leq \mathbf{x}_{1\mathbf{max}} & \text{(19-a)} \\ \mathbf{d_{ck}} \in [0,1] & \text{(19-b)} \\ \lambda\mathbf{I} - \mathbf{A}_1 = 0\ \mathrm{Re}(\lambda) \leq 0 & \text{(19-c)} \end{cases}$$

If the inequalities constraints are satisfied, continue to **Step 5**. Otherwise, go to **Step 7**.

Step 5: Output the current set of droop matrix **E**.

Step 6: Set $t = t + \Delta t$ to start a new round of calculations until a steady state is reached.

Step 7: Input a new set of droop gains to form an updated droop matrix **E**and start a new round of calculations.

Step 1-3 conduct the iterative calculations and determine whether the selected droop gains can meet the convergence criteria and reach a steady state with satisfactory performance, say within N_{max} and $T_{\max}$. The inequality constraints defined in **Step 4** assesses if the control performance meets the following requirements:

- (19-a) examines if the DC branch/line currents are operated within their maximum limits under steady state;
- (19-b) checks if the duty cycles of the switches, $\mathbf{d_{ck}}$ are controlled between 0 and 1;
- (19-c) assesses if system eigenvalues are all located in left-hand plane to satisfy the system stability requirement.

V. SIMULATION RESULTS

In order to evaluate the effectiveness of the proposed droop control scheme and droop gain selection method, a meshed 4-terminal VSC HVDC system is established on the real-time digital simulator (RTDS). For the simulation model, a full detailed model is used with considering the dynamics of the meshed MTDC grid and the VSC MMC dynamics. The configuration of the 4-terminal test system is depicted in Fig. 7. The system has 4 DC terminals and 5 DC branches/lines that interconnect these terminals. The decoupled *dq* control is utilized by the VSC converters for the DC voltage control and power regulation [37]. T_1, T_2 and T_4 use active power control

and reactive power control, while T_3 applies DC voltage control and reactive power control. Parameters of the DC branches/lines including the current limits that are simulated in the MTDC system are shown in Table 3 [31], [38], [39]. The inductance of the DC branches/lines is 0.07 mH/km and the capacitance is 0.05 μF/km [31], [38], [39]. The control settings of the VSCs are presented in Table 4. The multi-line CFC installed at T_1 is designed to control the currents on the DC branches/lines where it is installed, i.e. DC branch/line currents on B_{12}, B_{13}, B_{14}.

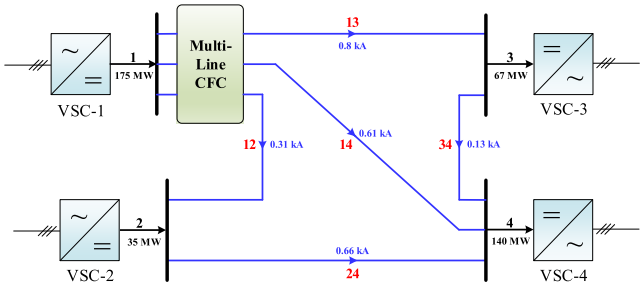

FIGURE 7. Configuration of a meshed 4-terminal HVDC test system.

TABLE 3. Parameters of the DC branches/lines.

Branches	B_{12}	B_{13}	B_{14}	B_{24}	B_{34}
Distance [km]	75	125	200	150	175
Resistance [Ω]	0.75	1.25	2.00	1.50	1.75
Current limits [kA]	1.20	1.20	1.20	1.00	0.60

TABLE 4. Control strategies and ratings of AC/DC terminals.

Terminals	T_1	T_2	T_3	T_4
VSC control strategy	*P, Q*	*P, Q*	V_{dc}, *Q*	*P, Q*
Rated power/voltage [MW/MVar/kV]	175, 0	35, 0	100, 0	140, 0

The modelling of the MTDC system is derived and the approach for the droop gain selection is described in Section IV and the Appendix. Two main factors are identified to have an impact on the selection range of the droop gains:

- The selection range of the droop gains may vary with changing of operating conditions of the MTDC, e.g. if the active power at T_4 varies, the selection range of droop gains will change accordingly. The main reason is that the operating conditions reflect the system status and are closely related with system state variables $\mathbf{x_1}$ and controlled inputs $\mathbf{u}$. The state variables and controlled inputs of the MTDC need to be set at the initial stage (**Step 1**). The changes of them will have a direct impact on the subsequent iterative calculations for droop gain selection.
- The selection range of the droop gains is influenced by the selection of the parameters of the *PI* controllers of the CFC, e.g. the selection range of possible droop gains will increase when the parameter *P* of the *PI* controllers decreases from 1 to 0.3. This is due to the fact that the settings of the *PI* controllers will affect their output $\mathbf{d_{ck}}$, the change of which will directly vary state matrix $\mathbf{A_1}$ and thereby influence the iterative calculations for droop gain selection.

In the simulation cases, $\mathbf{x_{c1ref}}$ are selected as [0.58, 0.58, 0.58, 3]. In $\mathbf{E}$, D_{12}, D_{13}, D_{14} are selected as [0.8, 0.8, 0.8]. In order to verify the control capability of DC branch/line currents of the multi-line CFC, 9 simulation cases with three operating conditions are studied: 1) changing of current references; 2) sudden disconnection of Branch 14; 3) sudden loss of T_4, so as to investigate the dynamic performance of the multi-line CFC with the coordinated droop control.

TABLE 5. Arrangements of 9 cases.

CFC Status / Incidents	No CFC	CFC with basic current control	CFC with droop control
Changing of current references	*Case 1*	*Case 2*	*Case 3*
Disconnection of Branch 14	*Case 4*	*Case 5*	*Case 6*
Sudden loss of T_4	*Case 7*	*Case 8*	*Case 9*

The arrangements of 9 cases are listed in Table 5. Among all the cases, the simulation systems used are categorized into 3 groups according to the objectives of comparisons.

- The simulation system for *Case 1*, *4*, *7* is the same and the multi-line CFC is not equipped.
- The simulation system for *Case 2*, *5*, *8* is the same, where the multi-line CFC is equipped with the basic current control.
- The simulation system for *Case 3*, *6*, *9* is the same, where the multi-line CFC is equipped with the coordinated droop control as proposed.

The basic current control for *Case 2*, *5*, *8* is that the DC-DC converters of the multi-line CFC on Branch 12 and Branch 14 regulate i_{12} and i_{14} respectively, while the DC-DC converter on Branch 13 control the capacitor voltage of the CFC. *Case 1-3* present the system performance with respect to changes of current references. *Case 4-6* present the response of DC branch/line currents to sudden disconnection of a DC branch. *Case 7-9* present the response of DC branch/line currents to sudden loss of a terminal.

Simulation results of *Case 1*, *Case 2* and *Case 3* are presented in Fig. 8, Fig. 9 and Fig. 10, respectively. Fig. 8 demonstrates the DC branch/line current flow of the MTDC grid under steady state condition, since the multi-line CFC is not equipped. The initial current flow is $i_{12} = 0.31$ kA, $i_{13} = 0.8$ kA, $i_{14} = 0.61$ kA. Fig. 9 demonstrates the DC branch/line current flow with the multi-line CFC. Initially, the CFC is bypassed and the distribution of branch current flow is same

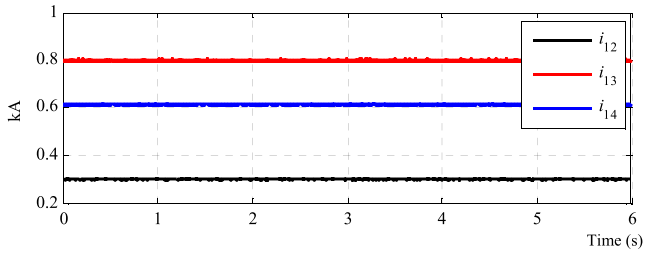

FIGURE 8. **Branch current flow of *Case 1*.**

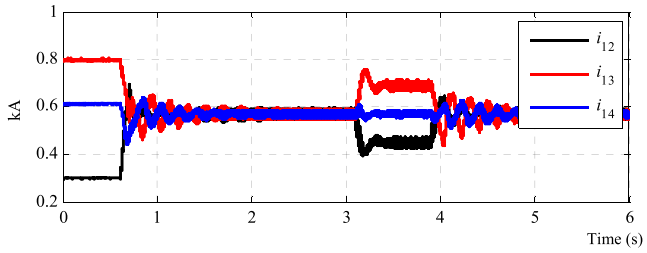

FIGURE 9. **Branch current flow of *Case 2*.**

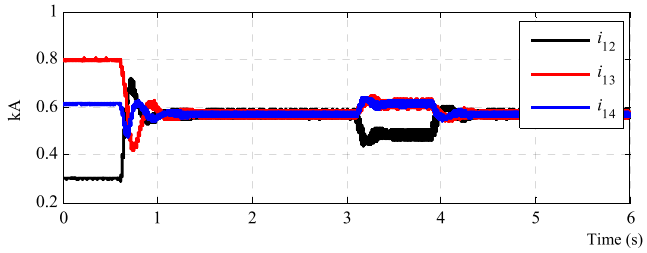

FIGURE 10. **Branch current flow of *Case 3*.**

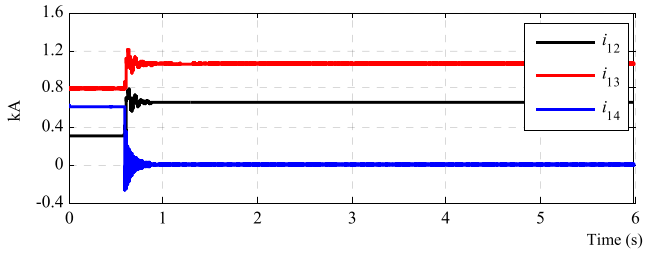

FIGURE 11. **Branch current response of *Case 4*.**

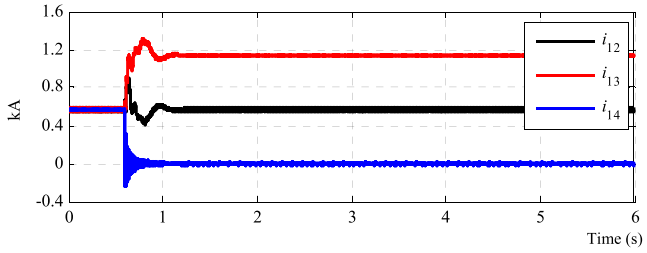

FIGURE 12. **Branch current response of *Case 5*.**

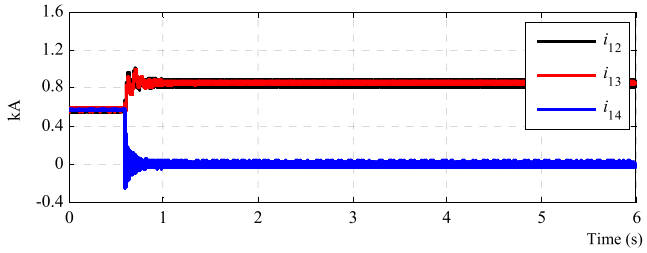

FIGURE 13. **Branch current response of *Case 6*.**

as that shown in Fig. 8. At 0.6 s, the CFC is activated and the branch currents are controlled to the same value of 0.58 kA. At 3.1 s, the current reference i_{12ref} is changed to 0.45 kA, i_{12} follows the current reference i_{12ref}. At 3.9 s, i_{12ref} returns the original current reference of 0.58 kA. It takes around 2 s for the DC branch/line currents to return the original steady state condition. Fig. 10 shows that when the CFC is activated at 0.6 s, i_{12}, i_{13} and i_{14} are controlled to be equal with a shorter transient in comparison with that shown in *Case 2*. When the current reference i_{12ref} is changed to 0.45 kA at 3.1 s and returns the original value at 3.9 s, i_{12} responses to both changes quickly and reaches the steady state within 0.5 s. The response of the DC branch/line currents in *Case 3* is faster and has fewer oscillations than those shown in *Case 2*.

Case 4-6 demonstrate the performance of the MTDC grid to a sudden disconnection of Branch 14 from the DC grid. Simulation results of *Case 4*, *Case 5* and *Case 6* are shown in Fig. 11, Fig. 12 and Fig. 13, respectively. Branch 14 is disconnected at 0.6 s. Fig. 11 demonstrates that the redistribution of DC branch/line currents between Branch 12 and Branch 13 is subject to the Ohm's law and is uncontrollable, since the CFC is not added. New steady state values of i_{12} and i_{13} are 0.7 kA and 1.1 kA respectively. The new steady state value of i_{13} becomes close to its transfer limit. Fig. 12 shows that the CFC achieves the control objective of regulating i_{12} to the reference value under the disturbance at 0.6 s. However, the new steady state value of i_{13} has a large increase. Fig. 13 shows that i_{12} and i_{13} are well controlled by the CFC and increase simultaneously to the same steady state value (0.87 kA). With the coordinated droop control, the multi-line CFC operates well under the disturbance and shares the current on the DC branch/line that is suddenly disconnected.

Case 7-9 demonstrate the performance of the MTDC grid to a sudden loss of T_4. Simulation results of *Case 7*, *Case 8* and *Case 9* are shown in Fig. 14, Fig. 15 and Fig. 16, respectively. Fig. 14 demonstrates that initially the system operates under steady state. At 0.6 s, T_4 is lost. The transient value of i_{13} increases swiftly and is up to 1.5 kA. In Fig. 15, significant current oscillations can be observed and current peak of i_{13} is over 1.2 kA during the loss of T_4. The multi-line CFC with the basic current control cannot perform its functionality under such a large disturbance. Fig. 16 demonstrates that although the loss of T_4 produces a large disturbance to the system, all the DC branch/line currents are controlled to less than 1 kA. With the coordinated droop control, the multi-line CFC performs the desired functionality and has the capability to

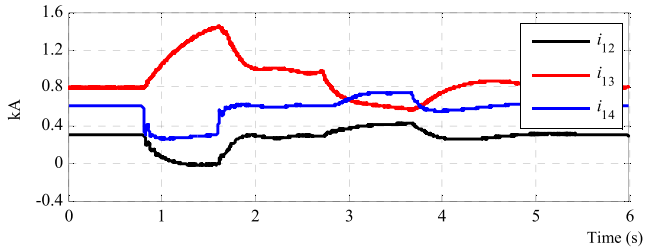

FIGURE 14. **Branch current response of *Case 7*.**

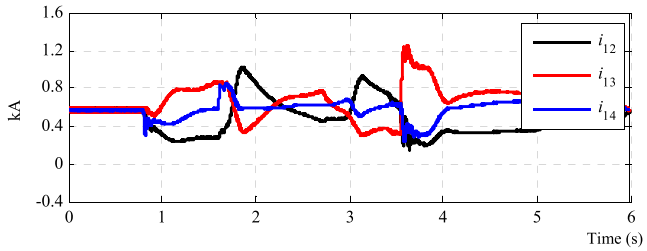

FIGURE 15. **Branch current response of *Case 8*.**

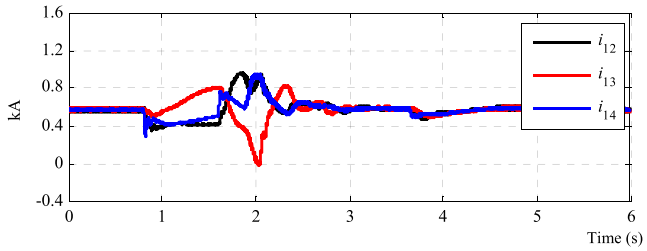

FIGURE 16. **Branch current response of *Case 9*.**

keep the DC branch/line currents within the limit under the large disturbance.

VI. CONCLUSION

A generalized modular and scalable multi-line CFC with for a MTDC grid have been expanded from the two-line CFC and presented in this paper. The major contribution has been focused on the coordinated droop control scheme and the associated droop gain selection for the multi-line CFC. The droop control scheme proposed has been justified to be capable of regulating multiple DC branch/line currents in meshed MTDC grids under both the steady states and DC disturbances. Based on the modelling and analysis of the MTDC grid with the multi-line CFC, a dynamic simulation based method for the droop gain selection has been proposed, which can fully consider the system nonlinear characteristics and control limits. In addition, two main factors that will have an impact on the selection range of the droop gains have been identified with explanation. The simulation results on the RTDS have justified the effectiveness of the proposed droop control scheme and the selection method for the droop gains. Comparison case studies have demonstrated that the use of droop control for the CFC has advantages over basic current control. In addition, regarding the feedback control algorithm and root-locus method, the selection method proposed has the superiority of less complexity and easier implementation, which improves the robustness of the droop controller. It has the merit of flexibility suiting both online and offline calculation tools. The multi-line CFC with the coordinated droop control proposed can operate well under large disturbances such as a sudden loss of a DC branch/line or a sudden loss of a DC terminal and hence can enhance the security, stability and reliability of DC grid operations.

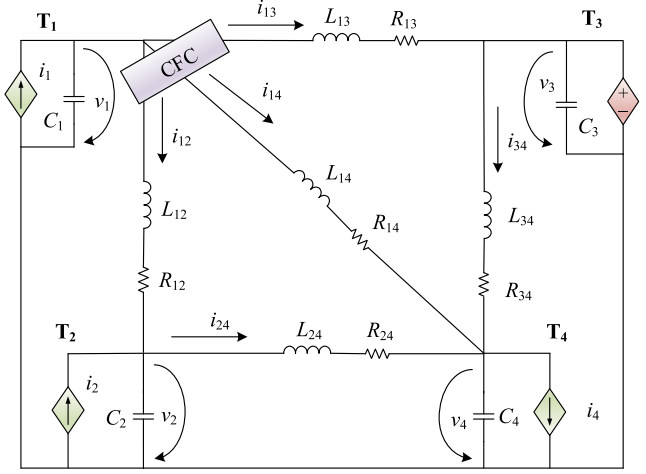

FIGURE 17. **Equivalent model of the test system.**

VII. APPENDIX

VIII. MODELLING AND DROOP GAIN SELECTION

An equivalent model of the testing system is shown in Fig. 17. By applying the Kirchhoff's voltage law (KVL) and Kirchhoff's current law (KCL) on the equivalent model in Fig. 17, systematic equations can be obtained as follows:

$$\begin{cases} \dfrac{dv_1}{dt} = \dfrac{1}{C_1}(i_1 - i_{12} - i_{13} - i_{14}) \\ \dfrac{dv_2}{dt} = \dfrac{1}{C_2}(i_2 + i_{12} - i_{24}) \\ \dfrac{dv_4}{dt} = \dfrac{1}{C_4}(i_{14} + i_{24} + i_{34} - i_4) \\ \dfrac{di_{12}}{dt} = \dfrac{1}{L_{12}}(v_1 - v_2 - R_{12}i_{12} - u_{c1}(d_{a1} - d_{c12})) \\ \dfrac{di_{13}}{dt} = \dfrac{1}{L_{13}}(v_1 - v_3 - R_{13}i_{13} - u_{c1}(d_{a1} - d_{c13})) \\ \dfrac{di_{14}}{dt} = \dfrac{1}{L_{14}}(v_1 - v_4 - R_{14}i_{14} - u_{c1}(d_{a1} - d_{c14})) \\ \dfrac{di_{24}}{dt} = \dfrac{1}{L_{24}}(v_2 - v_4 - R_{24}i_{24}) \\ \dfrac{di_{34}}{dt} = \dfrac{1}{L_{34}}(v_3 - v_4 - R_{34}i_{34}) \\ \dfrac{du_{c1}}{dt} = \dfrac{1}{C_{cfc}}(i_{12}(d_{a1} - d_{c12}) \\ \qquad + i_{13}(d_{a1} - d_{c13}) + i_{14}(d_{a1} - d_{c14})) \end{cases} \tag{20}$$

The state matrix $\mathbf{A_1}$ can be written as the equation can be derived, as shown at the top of the next page: The state vector

$$\mathbf{A_1} = \begin{bmatrix} 0 & 0 & 0 & -\frac{1}{C_1} & -\frac{1}{C_1} & -\frac{1}{C_1} & 0 & 0 & 0 \\ 0 & 0 & 0 & \frac{1}{C_2} & 0 & 0 & -\frac{1}{C_2} & 0 & 0 \\ 0 & 0 & 0 & 0 & 0 & \frac{1}{C_4} & \frac{1}{C_4} & \frac{1}{C_4} & 0 \\ \frac{1}{L_{12}} & -\frac{1}{L_{12}} & 0 & -\frac{R_{12}}{L_{12}} & 0 & 0 & 0 & 0 & -\frac{(d_{a1}-d_{c12})}{L_{12}} \\ \frac{1}{L_{13}} & 0 & 0 & 0 & -\frac{R_{13}}{L_{13}} & 0 & 0 & 0 & -\frac{(d_{a1}-d_{c13})}{L_{13}} \\ \frac{1}{L_{14}} & 0 & -\frac{1}{L_{14}} & 0 & 0 & -\frac{R_{14}}{L_{14}} & 0 & 0 & -\frac{(d_{a1}-d_{c14})}{L_{14}} \\ 0 & \frac{1}{L_{24}} & -\frac{1}{L_{24}} & 0 & 0 & 0 & -\frac{R_{24}}{L_{24}} & 0 & 0 \\ 0 & 0 & -\frac{1}{L_{34}} & 0 & 0 & 0 & 0 & -\frac{R_{34}}{L_{34}} & 0 \\ 0 & 0 & 0 & \frac{d_{a1}-d_{c12}}{C_{cfc}} & \frac{d_{a1}-d_{c13}}{C_{cfc}} & \frac{d_{a1}-d_{c14}}{C_{cfc}} & 0 & 0 & 0 \end{bmatrix}$$

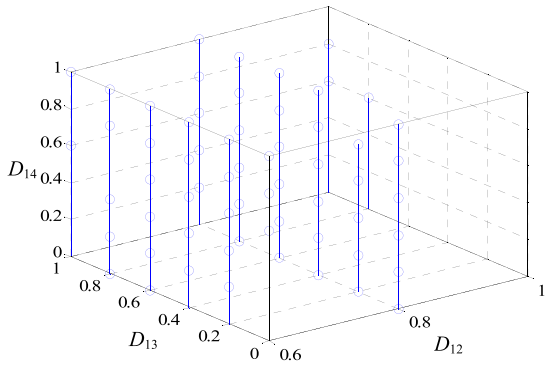

FIGURE 18. **Droop gain selection results.**

$\mathbf{x_1}$ can be written as:

$$\mathbf{x_1} = [v_1, v_2, v_4, i_{12}, i_{13}, i_{14}, i_{24}, i_{34}, u_{c1}]^T$$

The input vector u is:

$$\mathbf{u} = [i_1, i_2, v_3, i_4]^T$$

Based on (15), three equality constraints are derived. The expressions of $\mathbf{x_{c1}}$ and $\mathbf{x_{c1ref}}$ are:

$$\mathbf{x_{c1}} = [i_{12}, i_{13}, i_{14}, u_{c1}]^T$$
$$\mathbf{x_{c1ref}} = \left[i_{12ref}, i_{13ref}, i_{14ref}, u_{c1ref}\right]^T$$

In addition, inequality constraints are defined as:

$$\begin{cases} i_{12} \le i_{12\mathbf{max}},\ i_{13} \le i_{13\mathbf{max}},\ i_{14} \le i_{14\mathbf{max}} & \text{(21-a)} \\ 0 \le d_{c12} \le 1,\ 0 \le d_{c13} \le 1,\ 0 \le d_{c14} \le 1 & \text{(21-b)} \\ \lambda\mathbf{I} - \mathbf{A}_1 = 0,\ \mathrm{Re}(\lambda) \le 0 & \text{(21-c)} \end{cases}$$

$\mathbf{E}$ is the droop gain matrix, which can be written as:

$$\mathbf{E} = \begin{bmatrix} D_{12} & 0 & 0 & 1-D_{12} \\ 0 & D_{13} & 0 & 1-D_{13} \\ 0 & 0 & D_{14} & 1-D_{14} \end{bmatrix}$$

The selection ranges for the droop gains, D_{12}, D_{13} and D_{14} in $\mathbf{E}$ are obtained by using the method introduced in Section III-C. Fig. 18 presents the results of the droop gain selection. A scanning method is used for the selection of the droop gains where a step of 0.2 is chosen for the selection of the droop gains between [0, 1], yielding 6 points per droop gain. In total, 216 choices of $\mathbf{E}$ are evaluated. Nevertheless, the step length of 0.2 could be shortened to obtain more combinations and possibilities of droop gain selections.

ACKNOWLEDGMENT

P. Wang and N. Deng were with the Department of Electronic Electrical and Systems Engineering, School of Engineering, University of Birmingham, Birmingham, U.K.

REFERENCES

[1] X.-P. Zhang, "Multiterminal voltage-sourced converter-based HVDC models for power flow analysis," *IEEE Trans. Power Syst.*, vol. 19, no. 4, pp. 1877–1884, Nov. 2004.

[2] G. O. Kalcon, G. P. Adam, O. Anaya-Lara, S. Lo, and K. Uhlen, "Small-signal stability analysis of multi-terminal VSC-based DC transmission systems," *IEEE Trans. Power Syst.*, vol. 27, no. 4, pp. 1818–1830, Nov. 2012.

[3] A. Hiorns, R. Smith, and D. Wright, "An integrated approach to offshore electricity transmission," in *Proc. IET 9th Int. Conf. AC/DC Power Transmiss.*, London, U.K., Oct. 2010, pp. 1–5.

[4] T. M. Haileselassie and K. Uhlen, "Power system security in a meshed North Sea HVDC grid," *Proc. IEEE*, vol. 101, no. 4, pp. 978–990, Feb. 2013.

[5] J. Beerten and R. Belmans, "Analysis of power sharing and voltage deviations in droop-controlled DC grids," *IEEE Trans. Power Syst.*, vol. 28, no. 4, pp. 4588–4597, Nov. 2013.

[6] E. Veilleux and B.-T. Ooi, "Power flow analysis in multi-terminal HVDC grid," in *Proc. IEEE/PES Power Syst. Conf. Expo. (PSCE)*, Phoenix, AZ, USA, Mar. 2011, pp. 1–7.

[7] X.-P. Zhang, E. Handschin, and M. Yao, "Modeling of the generalized unified power flow controller (GUPFC) in a nonlinear interior point OPF," *IEEE Trans. Power Syst.*, vol. 16, no. 3, pp. 367–373, Aug. 2001.

[8] N. R. Chaudhuri and B. Chaudhuri, "Adaptive droop control for effective power sharing in multi-terminal DC (MTDC) Grids," *IEEE Trans. Power Syst.*, vol. 28, no. 1, pp. 21–29, Feb. 2013.
[9] Z. Shen and V. Dinavahi, "Comprehensive electromagnetic transient simulation of AC/DC grid with multiple converter topologies and hybrid modeling schemes," *IEEE Power Energy Tech. Syst. J.*, vol. 4, no. 3, pp. 40–50, Sep. 2017.
[10] J. Cao, W. Du, H. F. Wang, and S. Q. Bu, "Minimization of transmission loss in meshed AC/DC grids with VSC-MTDC networks," *IEEE Trans. Power Syst.*, vol. 28, no. 3, pp. 3047–3055, Aug. 2013.
[11] L. Xiao, Z. Xu, T. An, and Z. Bian, "Improved analytical model for the study of steady state performance of droop-controlled VSC-MTDC systems," *IEEE Trans. Power Syst.*, vol. 32, no. 3, pp. 2083–2093, May 2017.
[12] G. Stamatiou and M. Bongiorno, "Power-dependent droop-based control strategy for multi-terminal HVDC transmission grids," *IET Gen. Trans. Distrib.*, vol. 11, no. 2, pp. 383–391, Jan. 2017.
[13] K. Rouzbehi, A. Miranian, J. I. Candela, A. Luna, and P. Rodriguez, "Proposals for flexible operation of multi-terminal DC grids: Introducing flexible DC transmission system (FDCTS)," in *Proc. Int. Conf. Renew. Energy Res. Appl. (ICRERA)*, Milwaukee, WI, USA, Oct. 2014, pp. 180–184.
[14] Q. Mu, J. Liang, Y. Li, and X. Zhou, "Power flow control devices in DC grids," in *Proc. IEEE PES Gen. Meeting*, San Diego, CA, USA, Jul. 2012, pp. 1–7.
[15] D. Jovcic, M. Hajian, H. Zhang, and G. Asplund, "Power flow control in DC transmission grids using mechanical and semiconductor based DC/DC devices," in *Proc. 10th IET Int. Conf. AC/DC Power Transmiss.*, Birmingham, U.K., Dec. 2012, pp. 1–6.
[16] G. J. Kish and P. W. Lehn, "A modular bidirectional DC power flow controller with fault blocking capability for DC networks," in *Proc. IEEE 14th Workshop Control Modeling Power Electron.*, Salt Lake, UT, USA, Jun. 2013, pp. 1–7.
[17] G. J. Kish, M. Ranjram, and P. W. Lehn, "A modular multilevel DC/DC converter with fault blocking capability for HVDC interconnects," *IEEE Trans. Power Electron.*, vol. 30, no. 1, pp. 148–162, Jan. 2015.
[18] J. Yang, Z. He, H. Pang, and G. Tang, "The hybrid-cascaded DC–DC converters suitable for HVdc applications," *IEEE Trans. Power Electron.*, vol. 30, no. 10, pp. 5358–5363, Oct. 2015.
[19] D. Liu and H. Li, "A ZVS bi-directional DC–DC converter for multiple energy storage elements," *IEEE Trans. Power Electron.*, vol. 21, no. 5, pp. 1513–1517, Sep. 2006.
[20] L. Wang, Z. Wang, and H. Li, "Asymmetrical duty cycle control and decoupled power flow design of a three-port bidirectional DC-DC converter for fuel cell vehicle application," *IEEE Trans. Power Electron.*, vol. 27, no. 2, pp. 891–904, Feb. 2012.
[21] S. Wang, J. Guo, C. Li, S. Balasubramaniam, R. Zheng, and J. Liang, "Coordination of DC power flow controllers and AC/DC converters on optimising the delivery of wind power," *IET Renew. Power Gener.*, vol. 10, no. 6, pp. 815–823, Jul. 2016.
[22] E. Veilleux and B.-T. Ooi, "Multiterminal HVDC with thyristor power-flow controller," *IEEE Trans. Power Del.*, vol. 27, no. 3, pp. 1205–1212, Jul. 2012.
[23] T. Zhang, C. Li, and J. Liang, "A thyristor based series power flow control device for multi-terminal HVDC transmission," in *Proc. 49th Int. Univ. Power Eng. Conf. (UPEC)*, Cluj-Napoca, Romania, Sep. 2014, pp. 1–5.
[24] S. Balasubramaniam, J. Liang, and C. E. Ugalde-Loo, "An IGBT based series power flow controller for multi-terminal HVDC transmission," in *Proc. 49th Int. Univ. Power Eng. Conf. (UPEC)*, Cluj-Napoca, Romania, Sep. 2014, pp. 1–6.
[25] F. Xu and Z. Xu, "A modular multilevel power flow controller for meshed HVDC grids," *Sci. China Tech. Sci.*, vol. 57, no. 9, pp. 1773–1784, Sep. 2014.
[26] W. Chen, X. Zhu, L. Yao, X. Ruan, Z. Wang, and Y. Cao, "An interline DC power-flow controller (IDCPFC) for multiterminal HVDC system," *IEEE Trans. Power Del.*, vol. 30, no. 4, pp. 2027–2036, Aug. 2015.
[27] M. Ranjram and P. W. Lehn, "A multiport power-flow controller for DC transmission grids," *IEEE Trans. Power Del.*, vol. 31, no. 1, pp. 389–396, Feb. 2016.
[28] K. Rouzbehi, J. I. Candela, A. Luna, G. B. Gharehpetian, and P. Rodriguez, "Flexible control of power flow in multiterminal DC grids using DC-DC converter," *IEEE J. Emerg. Sel. Topics Power Electron.*, vol. 4, no. 3, pp. 1135–1144, Sep. 2016.
[29] C. D. Barker and R. S. Whitehouse, "A current flow controller for use in HVDC grids," in *Proc. IET 10th Int. Conf. AC/DC Power Transmiss.*, Birmingham, U.K., Dec. 2012, pp. 1–5.
[30] N. Deng, P. Wang, X.-P. Zhang, G. Tang, and J. Cao, "A DC current flow controller for meshed modular multilevel converter multiterminal HVDC grids," *CSEE J. Power Energy Syst.*, vol. 1, no. 1, pp. 43–51, Mar. 2015.
[31] N. Deng, P. Wang, and X.-P. Zhang, "Small-signal stability analysis and control system design of a meshed multi-terminal HVDC grid with a current flow controller," *Elect. Power Comp. Syst.*, vol. 44, no. 10, pp. 1126–1137, Jun. 2016.
[32] D. G. Holmes and T. A. Lipo, *Pulse width Modulation for Power Converters: Principles and Practice*, 1st ed. Hoboken, NJ, USA: Wiley, 2003.
[33] *Heun's Method*. Accessed: Jun. 10, 2018. [Online]. Available: https://en.wikipedia.org/wiki/Heun's_method
[34] *The Euler-Heun Method*. Accessed: Jun. 10, 2018. [Online]. Available: http://livetoad.org/Courses/Docu-ments/214a/Notes/euler-heun_method.pdf
[35] U. M. Ascher and L. R. Petzold, *Computer Methods for Ordinary Differential Equations and Differential-Algebraic Equations*, 1st ed. Pennsylvania, PA, USA: SIAM, 1998.
[36] C.-F. Fong, D. Kee, and P.-N. Kaloni, *Advanced Mathematics for Engineering and Science*, 1st ed. Singapore: World Scientific, 2003.
[37] P. Wang, X.-P. Zhang, P. F. Coventry, and R. Zhang, "Start-up control of an offshore integrated MMC multi-terminal HVDC system with reduced DC voltage," *IEEE Trans. Power Syst.*, vol. 31, no. 4, pp. 2740–2751, Jul. 2016.
[38] P. Bresesti, W. L. Kling, R. L. Hendriks, and R. Vailati, "HVDC connection of offshore wind farms to the transmission system," *IEEE Trans. Energy Convers.*, vol. 22, no. 1, pp. 37–43, Mar. 2007.
[39] S. Liu, Z. Xu, W. Hua, G. Tang, and Y. Xue, "Electromechanical transient modeling of modular multilevel converter based multi-terminal HVDC systems," *IEEE Trans. Power Syst.*, vol. 29, no. 1, pp. 72–83, Jan. 2014.

PUYU WANG (S'13–M'15) received the B.Eng. degree in electrical engineering from the Huazhong University of Science and Technology, China, and the University of Birmingham, U.K., in 2011, and the Ph.D. degree from the University of Birmingham, Birmingham, U.K., in 2016. From 2013 to 2016, he was a Research Fellow in electrical power systems with the University of Birmingham. He is currently a Lecturer with the Department of Electrical Engineering, School of Automation, Nanjing University of Science and Technology, China. His research interests include HVDC technology, dc–dc converters, grid integration of renewable energy, and power electronics applications in power systems.

NA DENG received the B.Eng. degree from the Huazhong University of Science and Technology, China, in 2011, and the Ph.D. degree from the University of Birmingham, U.K., in 2015. From 2014 to 2015, she was a Bond Engineer with GE/Alstom Grid, U.K. In 2015, she joined ABB Sifang Power System Co., Ltd., China, as a System Engineer and transferred to ABB (China) Ltd., in 2017, where she is currently a R&D Engineer. Her research interests include HVDC technology, dc–dc converters, microgrids, and general applications of power electronics in power systems.

XIAO-PING ZHANG (M'95–SM'06) received the B.Eng., M.Sc., and Ph.D. degrees from Southeast University, China, in 1988, 1990, and 1993, respectively, all in electrical engineering. He was an Associate Professor with the University of Warwick, U.K. He was with the China State Grid EPRI (NARI Group) on EMS/DMS advanced application software research and development from 1993 to 1998. From 1998 to 1999, he was visiting UMIST. From 1999 to 2000, he was an Alexander-von-Humboldt Research Fellow with the University of Dortmund, Germany. He is currently a Professor of electrical power systems with the University of Birmingham, U.K., and also the Director of Smart Grid, Birmingham Energy Institute, and the Co-Director of the Birmingham Energy Storage Center. He has co-authored the monograph *Flexible AC Transmission Systems: Modeling and Control* (Springer first edition, 2006 and second edition, 2012). He has co-authored the book "*Restructured Electric Power Systems: Analysis of Electricity Markets with Equilibrium Models*" (IEEE Press/Wiley, 2010). He has been a Pioneer in promoting the concept of "Energy Quality", "Global Power & Energy Internet," "Energy Union," and "U.K.'s Energy Valley."